POST-PEAK CYCLIC BEHAVIOR AND DUCTILITY OF REINFORCED CONCRETE COLUMNS

Rajesh P. Dhakal[1] and Koichi Maekawa[2]

Abstract

This study aims to bring into information some important aspects of the inelastic cyclic response of reinforced concrete columns. Here, the behavior of reinforced concrete columns under lateral cyclic loading is studied using a three-dimensional finite element analysis program. It consists of path dependent and nonlinear constitutive models representing the stress-strain relationships of the constituent materials. Inelastic material behaviors, such as cover concrete spalling and large lateral deformation of buckled reinforcement, which influence the post-peak inelastic response of RC columns, are modeled and included in the material models. Some experiments conducted by the authors and other researchers are adopted for the verification and discussion of the analytical results. Reasonable agreement between the analytical prediction and the experimental result is observed. In addition, importance of cover concrete spalling and reinforcement buckling is realized and their contribution to the overall post-peak response is assessed. A reinforced concrete column subjected to ground acceleration is analyzed and the seismic response of the column is also discussed.

Introduction

Recently, performance based design method is being widely discussed for reinforced concrete structures. Structures expected to be exposed to ground motion are designed according to their ductility and for such structures, the post-peak information is required to check the structural performance. Although 2D analysis can satisfactorily predict the response and ductility of pure 2D RC columns and shear walls, 3D analysis is a must for checking seismic performance of 3D RC columns with side reinforcements, the response of which will be over-estimated by 2D analysis. 3D diagonal shear crack profile develops in such columns and 3D crack

[1] Graduate Student, Dept. of Civil Engrg., University of Tokyo, Tokyo 113-8656, Japan.
[2] Professor, Dept. of Civil Engrg., University of Tokyo, Hongo, Tokyo 113-8656, Japan.

analysis is required for reliable prediction of capacity and ductility. Moreover, in order to consider the multidirectional loading due to ground motion also, 3D analysis is inevitable.

Reinforced concrete columns subjected to cyclic loading or ground motion often experience high deformation and the load-displacement relationship frequently reaches the post-peak range. From the results of various experiments conducted in the past on laterally loaded reinforced concrete columns, considerable softening phenomenon can be distinguished in the load-displacement relationship in the inelastic region [Fukui et al., 1998]. It has been realized in the past that this inelastic softening behavior is mainly due to the spalling of cover concrete and buckling of longitudinal reinforcement [Suda et al. 1996]. These mechanisms significantly influence the deformation capacity and ductility of the structure. The additional softening, due to spalling of cover concrete and buckling of reinforcement, causes significant difference in the ultimate displacement capacity. Consequently, if this inelastic softening behavior is overlooked in the analysis, the ductility is overestimated. The torsion resistance of RC column is also over-estimated if the diagonal cover concrete spalling is neglected. Hence, the cover spalling and reinforcement buckling should be paid due attention in the analysis.

In the past, comparatively more attention was paid to the analytical prediction of pre-peak response and the reliability of post-peak prediction was compromised to a great extent. Through this study, the authors have attempted to understand the material mechanisms involved especially in the inelastic behavior of laterally loaded reinforced concrete columns. In addition, it is tried to enhance the analytical models by simulating and incorporating these highly inelastic material mechanisms in the material constitutive relationships so that the reliability of analytical prediction of inelastic response is improved. In order to achieve the mentioned goals, some lateral loading experiments are conducted on reinforced concrete columns and analyses of those structural members are performed.

Analytical Models

A three-dimensional finite-element analysis program called COM3 (*Co*ncrete *M*odel in *3*D), developed in Concrete Laboratory, The University of Tokyo, is used for the analytical prediction of the behavior of RC columns. It includes nonlinear and path-dependent material constitutive models applicable to loading, unloading and reloading conditions as well. They have been verified in the element and member levels with satisfactory results, and have been incorporated in the FEM program for the analysis of reinforced concrete under monotonic and cyclic loading [Okamura and Maekawa 1991]. However, the effect of spalling of cover concrete and the large lateral deformation of reinforcement are not incorporated in the path-dependent nonlinear models. These phenomena can be commonly observed in real structures and small-scale experiments subjected to ground motion. It is thought that these phenomena would have much to do with the inelastic response and should not be ignored especially in analysis of the structures designed for high ductility, as these

structures may be subjected to higher strains. In order to study the effect of these mechanisms, the spalling of cover concrete and buckling of reinforcement are modeled and incorporated in COM3 to analyze reinforced concrete columns.

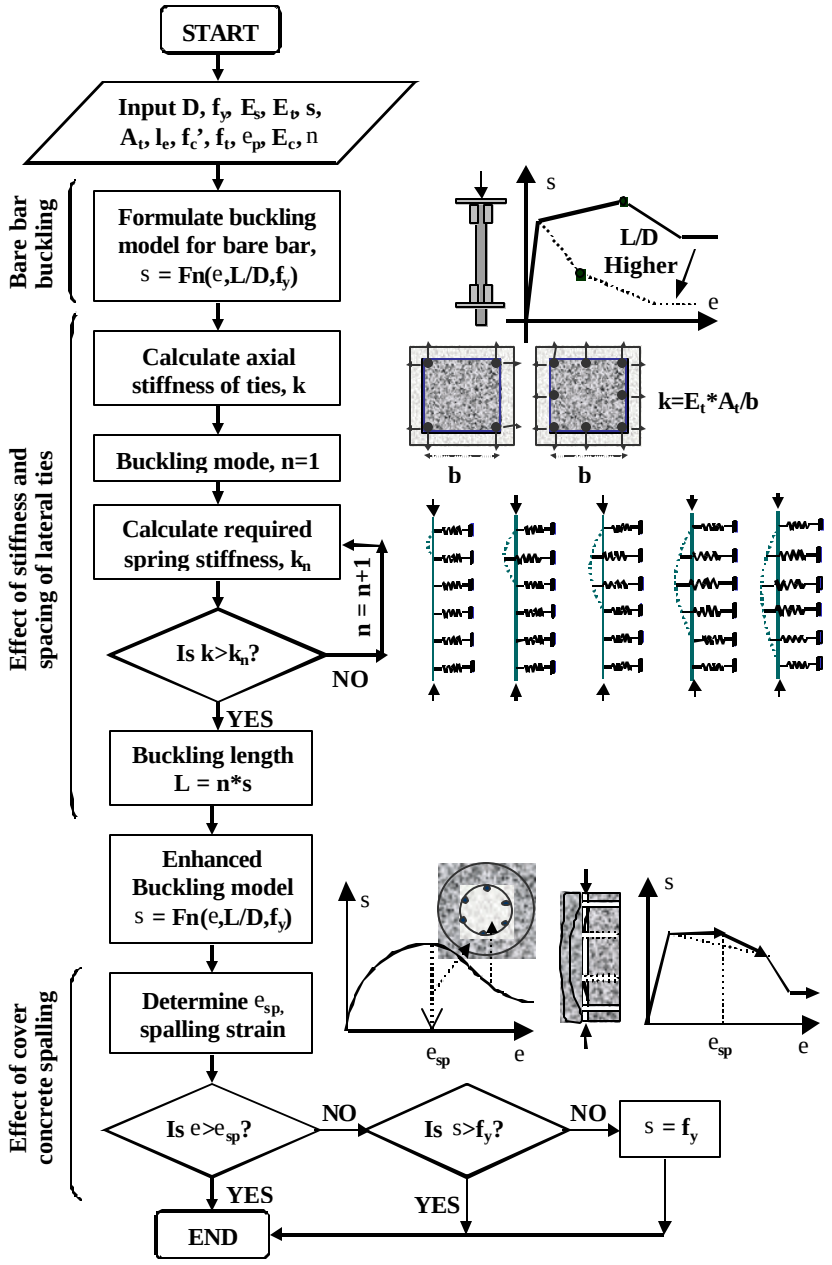

FIGURE 1. Formulation of compressive stress-strain relationship of reinforcement

Reinforcing bars in RC members, when subjected to high compressive strain, undergo large lateral deformation. This behavior is referred to as buckling of reinforcement and is mainly associated with high geometrical nonlinearity. However, in this study, this mechanism is implicitly incorporated in the material model of reinforcing bars. The formulation of stress-strain relationship of reinforcement fibers

in reinforced concrete structures is explained with the help of a flow chart and illustrations as shown in figure 1. The entire process comprises of three parts; formulation of bare bar buckling model, effect of lateral ties and effect of cover concrete spalling. These three components are separately described hereafter. A compressive stress-strain relationship is proposed based on the facts observed by previous researches [Monti and Nuti 1992, Mau and El-Mabsout 1989] related to bare bar buckling mechanism. Nevertheless, such constitutive relations of the bare bar cannot be directly applied to the reinforcing bars inside reinforced concrete members. For practical application in reinforced concrete structures, these relations need to be enhanced by considering various interrelated mechanisms, which affect the large lateral deformation of reinforcement. Spalling of cover concrete and geometrical and mechanical properties of lateral ties are thought to have significant influence on the geometrical nonlinearity of reinforcement and these factors should be incorporated in the buckling model. But, comparatively fewer researches in the past [Suda 1998] have addressed the integration of cover concrete spalling and buckling behavior of longitudinal reinforcements supported laterally by a system of transverse reinforcements (stirrups) inside structures. In this study, both spalling and buckling models are integrated and used in the analysis. The integrated model is verified and its application to the reinforced concrete structures is also discussed.

Buckling Model of Bare Bar

In the past, various experimental and analytical studies have been done on the buckling of bare reinforcing bars under compression [Mau 1990, Gomes and Appleton 1997, Rodriguez et al. 1999]. Through these studies, it has been understood that the stress-strain relationship of reinforcing bar follows an elastic path until compression yielding is reached. After compression yielding, the stress-strain relationship shows slight hardening followed by softening behavior. It can be observed that the hardening stiffness and the strain at the starting point of softening depend on the length to diameter ratio of the test bar [Monti and Nuti 1992]. The stress-strain relationship is also affected by the yield strength of the bar. It is found that the increase in the yield stress increases the hardening stiffness, decreases the hardening range and makes the response more brittle [Mau and El-Mabsout 1989].

Based on this information, a trilinear post-yielding compressive stress-strain relationship for bare bar is proposed. After the yielding strain in compression is reached, stiffness is determined depending on the bar yield strength and the bar length to bar diameter ratio. The inelastic softening behavior, induced by buckling mechanism, is also modeled according to the yield strength and the length to diameter ratio. For unloading and reloading behavior in a cyclic loop, a smooth transition curve asymptotic to the tangents at the point of stress reversal and the point of maximum/minimum strain in the loading history, as proposed by Giuffre-Menegotto-Pinto [CEB 1996], is used. The monotonic and cyclic models of bare bar are shown in figure 2.

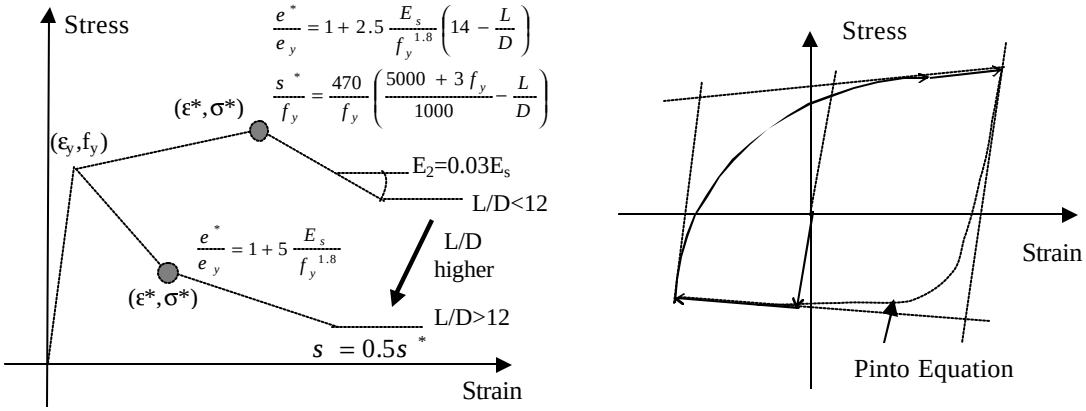

FIGURE 2. Monotonic and cyclic buckling models.

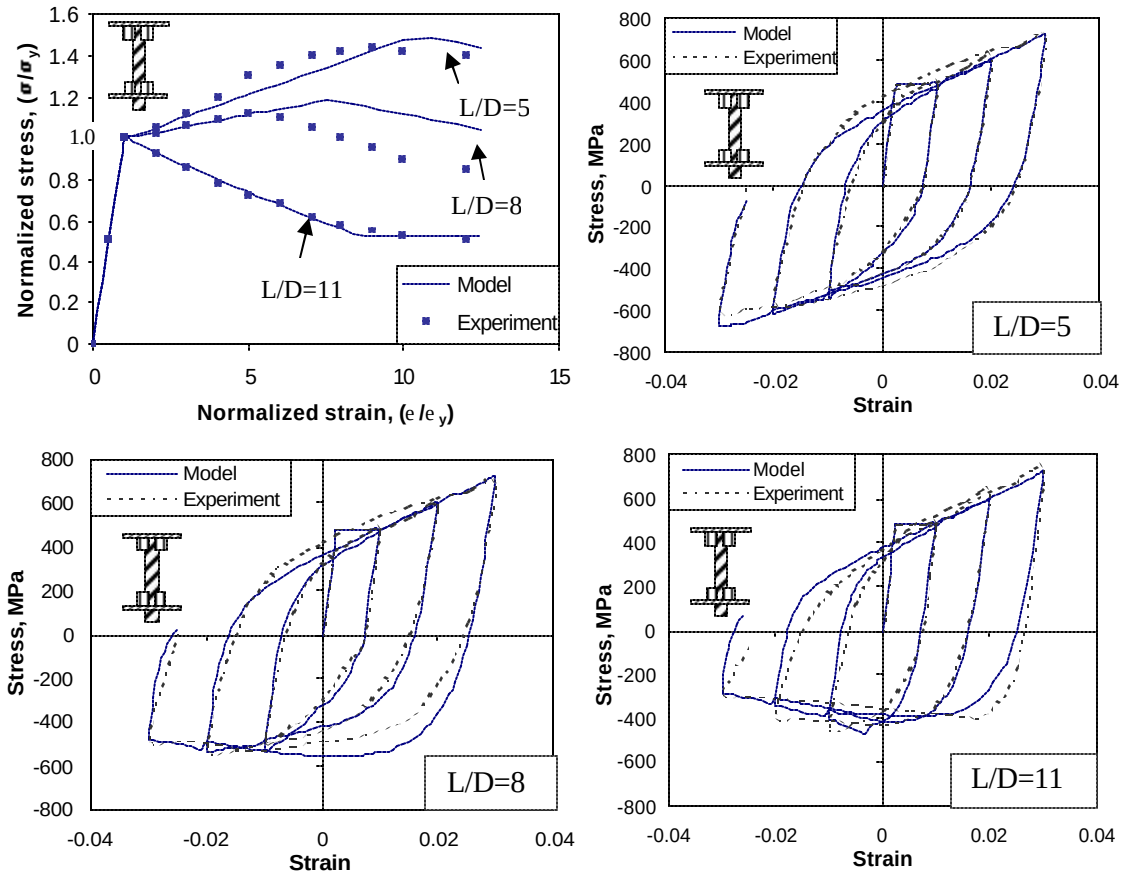

FIGURE 3. Model verification for monotonic and cyclic cases.

The proposed models are compared with the experimental results [Monti and Nuti 1992] and the comparison is illustrated in figure 3. The experiment consists of series of monotonic and cyclic tests on steel bars with different *L/D* ratio. It can be observed that the proposed model is in good agreement with the experimental results, both for monotonic and cyclic behaviors of reinforcing bars with different slenderness

ratio. It is found that the lower the *L/D* ratio is, the buckling effect decreases. For *L/D* ratio equal to 5, buckling effect nearly diminishes and the response becomes the same as that in tension. Moreover, the cyclic response of reinforcement in tension is independent of *L/D* ratio and the extent of buckling attained in the past.

Buckling Length of Reinforcement

The most important parameter that governs the stress-strain relationship of reinforcing bar in compression is length to diameter ratio. In the compression tests of bare bar, the buckling length is equal to the supported length of the test piece. But for the reinforcing bars inside reinforced concrete structures, this definition of buckling length does not apply. Hence, the determination of length to diameter ratio, in such cases, becomes difficult and requires proper consideration of interrelated mechanisms between main bar and lateral ties.

Previous researchers [Bresler and Gilbert 1961, Scribner 1986] have adopted some contradictory assumptions regarding the buckling length. Bresler and Gilbert assumed that the lateral ties are sufficiently rigid to prevent the lateral displacement of the main bar at the level of the tie and replaced the buckling length with tie spacing. In contrast, Scribner reported that the plastic hinge in members subjected to repeated reverse inelastic flexure spans through a length equal to overall beam depth. By assuming that the distance between the consecutive ties is equal to one-quarter of the beam depth, it was concluded that the buckling length extends through the length equal to three times tie spacing. However, the reality seems to be different. Kato [Kato et al. 1995], in the experiments consisting of compression tests of reinforced concrete columns, observed that the buckling length varies from one to several times the tie spacing, depending on the geometrical and mechanical properties of the ties and main bar.

It is realized that the buckling length may extend to several tie spacings depending on the arrangement and strength of lateral ties. If the size and spacing of the lateral ties are designed properly so that the stiffness of the stirrup is high enough to provide a rigid support to the longitudinal bar, it is ensured that the main reinforcement buckles between two adjacent stirrups. It is to be noted that if buckling length changes from one to two times tie spacing, the length to diameter ratio is doubled. Consequently, the reinforcement stress-strain relationship in compression is significantly changed. Hence, response of reinforcing bars is very sensitive to the buckling length, which is equal to the integral multiple of tie spacing in such a discrete system. Simplified assumptions or a small difference between projected and actual values of buckling length might lead to significantly inaccurate reinforcement behavior. Here, a theoretical method to determine the buckling length is proposed.

The lateral ties are simulated by discrete elastic springs. The stiffness required by the spring, in order to prevent the lateral displacement of main bar at spring position, is calculated using the energy principle. This stiffness is compared with the actual stiffness of the lateral tie to determine whether the given strength and spacing

of the ties are sufficient enough to hold the main bar in the first buckling mode, i.e. buckling length equal to tie spacing, or not. If the tie stiffness is less than the required spring stiffness, then required spring stiffness for the next mode is calculated and compared with tie stiffness. The same procedure is followed until a stable buckling mode is reached so that the required stiffness of spring is less than the actual stiffness of lateral tie. The product of this stable buckling mode and the tie spacing gives the potential buckling length of the main reinforcement for the given arrangement of the lateral ties. This buckling length is used to calculate *L/D* ratio, instead of the spacing of the stirrups.

The derivation of required spring stiffness for an arbitrary mode (n^{th} mode) is explained below. Figure 4 presents the two possible modes of deformation (*n* and *n+1*) considered for the derivation. Here, we have to consider these two modes because we want to assess the spring stiffness so that the higher mode (*n+1*) is avoided. The lower modes are not considered because they are already checked in the previous steps and proved not to exist. To define the deformational shape of the reinforcement, boundary conditions ensuring zero lateral displacement and no slope at the end springs, are assumed. To fulfill these boundary conditions, a cosine curve (normally used for deformation of fixed end column) is used for each mode and the total deformation of the entire system is given by the sum of the constituent modes.

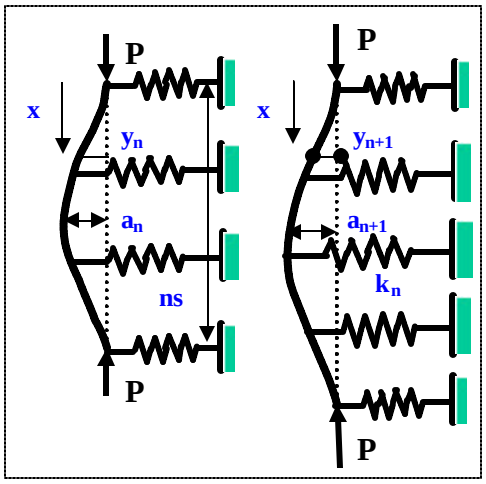

$$y_n = \frac{a_n}{2}\left(1-\cos\frac{2px}{ns}\right)$$

$$y_{n+1} = \frac{a_{n+1}}{2}\left(1-\cos\frac{2px}{(n+1)s}\right)$$

$$y = y_n + y_{n+1}$$

FIGURE 4. Calculation of required spring stiffness.

The total energy of the system includes the elastic strain energy of the reinforcement, energy stored in the elastic springs, and the energy due to shortening of the reinforcement. Hence, the total energy associated with the system *U* can be written as

$$U = \int_0^{(n+1)s} \frac{EI}{2}\left(\frac{d^2y}{dx^2}\right)^2 dx + \sum_{i=1}^{n} \frac{k_n}{2} y_n^{is\,2} + \sum_{i=1}^{(n+1)} \frac{k_n}{2} y_{n+1}^{is\,2} - \int_0^{(n+1)s} \frac{P_n}{2}\left(\frac{dy}{dx}\right)^2 dx$$

$$U = U_f + U_k - U_P$$

Here, U_f, U_k and U_P are the flexural strain energy of the reinforcement, energy stored in the elastic springs and the energy due to the shortening of the reinforcement, respectively. Similarly, EI is the flexural stiffness of the reinforcement and k_n and P_n are the critical spring stiffness and the axial load corresponding to the n^{th} mode, respectively. By solving these equations in using the pre-described deformational shape, we have

$$U_f = \frac{p^4 EI}{s^3}\left[\frac{a_n^2}{n^3} + \frac{a_{n+1}^2}{(n+1)^3} + \frac{a_n a_{n+1}}{n(n+1)(2n+1)p}\sin\frac{(2n+1)2p}{(n+1)} + \frac{a_n a_{n+1}}{n(n+1)p}\sin\frac{2p}{(n+1)}\right]$$

$$U_k = \frac{k_n a_n^2}{8}\sum_{i=1}^{n}\left(1-\cos\frac{2ip}{n}\right)^2 + \frac{k_n a_{n+1}^2}{8}\sum_{i=1}^{n+1}\left(1-\cos\frac{2ip}{(n+1)}\right)^2$$

$$U_P = \frac{p^2 P_n}{4s}\left[\frac{a_n^2}{n} + \frac{a_{n+1}^2}{n+1} + \frac{a_n a_{n+1}}{p}\sin\frac{2p}{n+1} - \frac{a_n a_{n+1}}{(2n+1)p}\sin\frac{(2n+1)2p}{(n+1)}\right]$$

As explained by the following equations, the total energy of the system, U, is minimized with respect to each of the maximum amplitudes, a_n and a_{n+1}.

$$\frac{\partial U}{\partial a_n} = 0 \Rightarrow \frac{\partial U_f}{\partial a_n} + \frac{\partial U_k}{\partial a_n} - \frac{\partial U_P}{\partial a_n} = 0$$

$$\frac{\partial U}{\partial a_{n+1}} = 0 \Rightarrow \frac{\partial U_f}{\partial a_{n+1}} + \frac{\partial U_k}{\partial a_{n+1}} - \frac{\partial U_P}{\partial a_{n+1}} = 0$$

Here, we get two linear equations including P_n and k_n as the variables. However, the coefficients consist of maximum amplitudes of both modes because of the presence of the higher order terms. In case of the first mode, these higher order terms do not matter because the trigonometric functions, which multiplies these higher order terms, turn out to be zero. But for higher modes, these terms do not vanish and create a numerical problem. For numerical simplicity, two options are considered here. The first is to neglect these terms and the second is to assume that the maximum amplitudes of the two adjacent modes are equal. It is found that both of these assumptions lead to almost similar results. Hence, the second assumption, i.e. equal maximum amplitudes for two consecutive modes, is used hereafter because it seems more rational than the first assumption. These two linear equations, now can be solved to get buckling load P_n and the required spring stiffness k_n.

TABLE 1. Required spring stiffness for different buckling modes

Buckling mode, n	1	2	3	4	5	6	7	8	9
Equivalent stiffness, k_{eq}	0.7500	0.2777	0.0488	0.0179	0.0080	0.0041	0.0023	0.0014	0.0009

The critical spring stiffness required for different buckling modes, calculated according to the proposed method, is shown in table 1. The equivalent stiffness (k_{eq}), mentioned in the table, is a dimensionless parameter. If k_{eq} is multiplied by p^4EI/s^3, the actual required stiffness can be obtained. As expected, the required spring stiffness becomes smaller for higher buckling modes. Hence, a stable buckling mode can be achieved for any arrangement of stirrups.

In order to determine the stable buckling mode and buckling length, the actual stiffness of the stirrups with given strength and arrangement, has to be evaluated in advance and it should be compared with the calculated required spring stiffness for the corresponding mode. The calculation of actual stiffness of stirrup is illustrated in figure 5. As shown in the figure, the buckling tendency of the main reinforcement will cause axial tension in the legs of stirrups. Hence, the stirrup resistance against the lateral expansion is believed to be mainly governed by the axial stiffness of the stirrups. The axial stiffness can be easily calculated using the elastic modulus (E_t), cross-sectional area (A_t) and the length of longer leg of the rectangular stirrup (b). For circular and spiral ties, the side length of equivalent square should be used. In case of multi-legged stirrups, the effective length of the stirrup leg should be calculated as explained in figure 5.

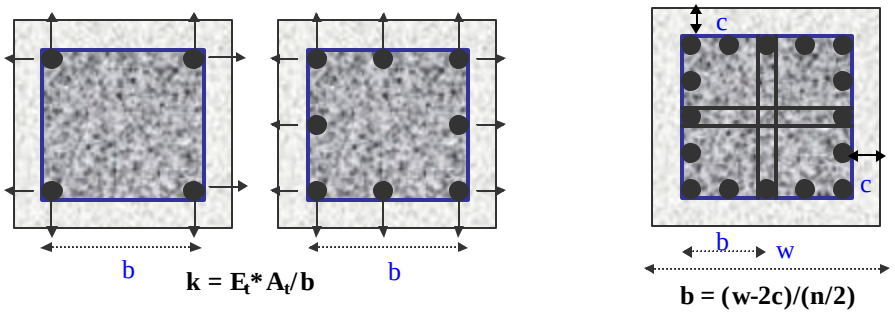

FIGURE 5. Calculation of axial stiffness of stirrup.

In reality, the lateral ties show elasto-plastic behavior and after reaching the yield strain, the stiffness of the tie is considerably reduced. To cope with this fact, the corresponding springs should be eliminated from the system for accurate prediction of required stiffness of other elastic springs. Because of the difficulty in evaluating the lateral displacements, this effect is not explicitly considered. However, the relative effect is investigated by neglecting the springs at the position of maximum displacement and all springs except at the two ends, respectively. It is found that the elimination of all springs, which is the extreme case, overestimates the required stiffness of the critical spring but the elimination of spring at maximum displacement does not influence the result so much. Hence, it is fairly assumed that the lateral springs are in the elastic range.

The proposed analytical method to predict buckling length of reinforcement is compared with the buckling lengths observed during experiments [Bresler and Gilbert 1961, Scribner 1986, Kato et al. 1995]. These experiments include the compression tests of reinforced concrete prisms and bending tests of reinforced concrete beams.

The comparison is presented in figure 6. As can be seen in the illustration, the proposed method is in fair agreement with the experimental observations. Hence, it can be concluded that this model can be reliably used for the design of lateral ties to resist extensive buckling of main reinforcement. Furthermore, this model can also be applied for continuous systems such as steel fiber reinforced concrete (SFRC). The buckling length can be determined based on the first mode and it was found that the delay in buckling behavior in SFRC could well be predicted.

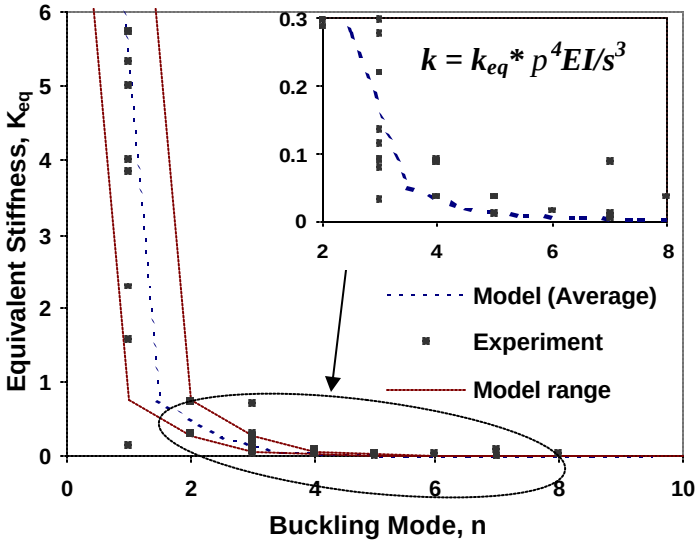

FIGURE 6. Verification of buckling length prediction method.

Effect of Cover Spalling

Reinforced concrete structures exhibit the spalling of cover concrete prior to the buckling of longitudinal reinforcement. The cover concrete loses the load carrying capacity after a limiting value of compressive strain is reached. The determination of spalling strain is explained in figure 7.

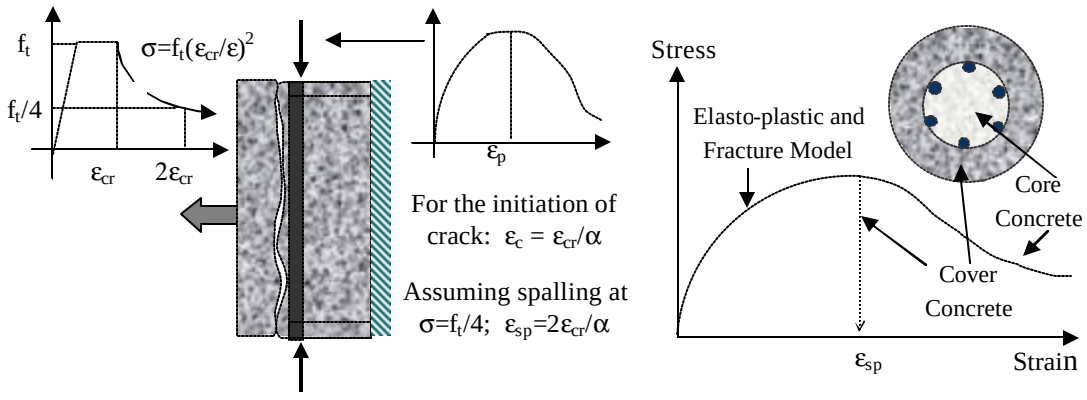

FIGURE 7. Spalling criteria for cover concrete.

Axial compression in the cover concrete induces tensile strain in the lateral direction. These two orthogonal strains are assumed to be related to each other by a factor a, equal to 0.2. Splitting cracks initiate after the induced lateral tensile strain reaches cracking strain. But, the concrete can still resist some axial tension due to the tension-softening behavior. The cover concrete can be treated as plain concrete in lateral direction and a tension softening factor c equal to 2 is assigned. The load resisting mechanism of the cracked concrete is neglected after the stress in the softening region becomes equal to 25% of the tensile strength. The tensile strain at this stage is found to be two times the cracking strain. The corresponding compressive strain, i.e. spalling strain, is calculated using factor a and it is found to be nearly equal to the peak strain of concrete. This model can satisfactorily explain the steel fiber reinforced concrete (SFRC) behavior, which doesn't easily show complete cover spalling. For SFRC, the tension softening factor c is smaller and consequently the spalling strain calculated by this model is very high, which is rarely experienced in actual loading.

Therefore, for the spalling of cover concrete, strain based criterion is used. Concrete in the cross-section is divided into two parts. The concrete portion outside the lateral reinforcement is modeled as cover concrete and the rest as core concrete. Once the compressive strain in the cover concrete exceeds the spalling strain, the stress transferred by cover concrete is reduced to zero. The buckling of reinforcement can occur only after spalling of the cover concrete. At this stage, the core concrete provides lateral support to the reinforcement so that the reinforcement buckles outwards, where the cover concrete is already spalled off. In order to cope with the fact that spalling precedes buckling, the reinforcement buckling model is modified so that the compressive stress-strain relationship does not undergo softening before the surrounding cover concrete is completely spalled out. Due to the compatibility condition, it can be said that if the strain in the reinforcement reaches the spalling strain, the surrounding cover concrete will spall out. After cover spalling, the reinforcement follows the bare bar stress-strain relationship.

Verification at Member Level

Experimental Setup and Analytical Simulation

Some experiments were conducted to study the behavior of laterally loaded reinforced concrete cantilever columns. The experimental setup and the specimen layout are shown in figure 8. Rectangular columns were cast monolithically with rigid footings and were subjected to cyclic lateral displacement. A triaxial loading machine was used so that axial and lateral loading could be applied simultaneously. In order to make the column function as a cantilever beam; the footing was tightly fixed to the base slab using prestressed tendons. The footings and the connection were designed to be rigid enough to provide a fixed support to the columns. Intended axial compression was applied at the top of the column and cyclic lateral displacement was applied at a height of 1200 mm from the top of the footing. For columns under axial compression, the P-delta effect is influential to the lateral load-displacement

relationship. Hence, proper geometrical nonlinearity as shown in figure 8, depending on the experimental setup, is also considered in the finite element analysis.

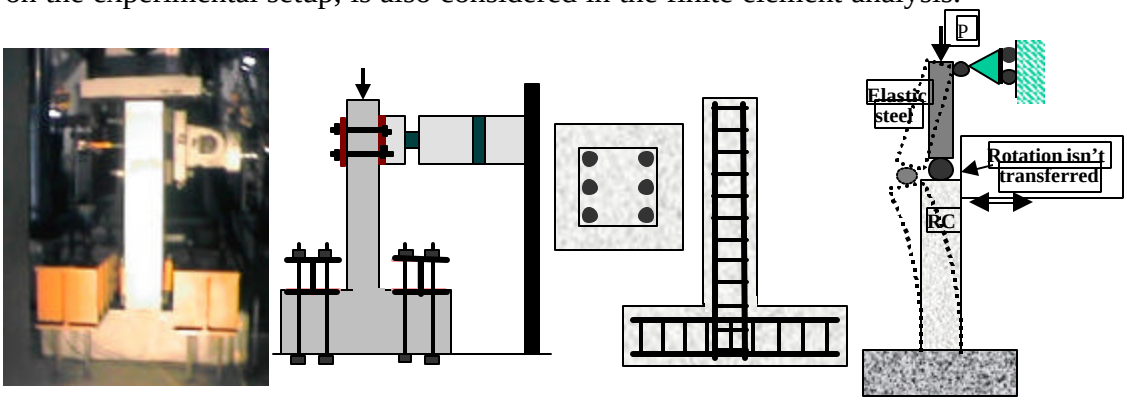

FIGURE 8. Experimental setup and geometrical nonlinearity in analysis.

Performance of Existing Models without Spalling and Buckling

To check the reliability of existing models for small displacement, an experiment was conducted so that the response does not reach the post-peak inelastic range. The experimental parameters are presented in table 2 and the results are depicted in figure 9. Small residual displacement was observed due to the significantly large cover, relatively lower reinforcement ratio and larger axial compression [Dhakal and Maekawa 1999].

As expected, the inelastic material mechanisms like cover concrete spalling and reinforcement buckling did not occur, as the response does not reach the peak. From the figure, it is clear that the existing models can predict the pre-peak behavior well. The analysis was performed with both three-dimensional solid elements and fiber technique. The analytical results with fiber technique and full 3-dimensional analysis are very close to each other, giving ample proof that fiber technique can be reliably used.

TABLE 2. Experimental parameters

Column cross section	250mm×250mm
Main reinforcement	6 no. D10 bars
Stirrups	D6 @100mm c/c
Cover thickness	80 mm
Axial compression	250 kN
Shear span	1200 mm
Compressive strength, f_c'	30 MPa
Tensile strength, f_t	2.5 MPa
Young's Modulus, E_s	197000 MPa
Yield strength, f_y	350 MPa

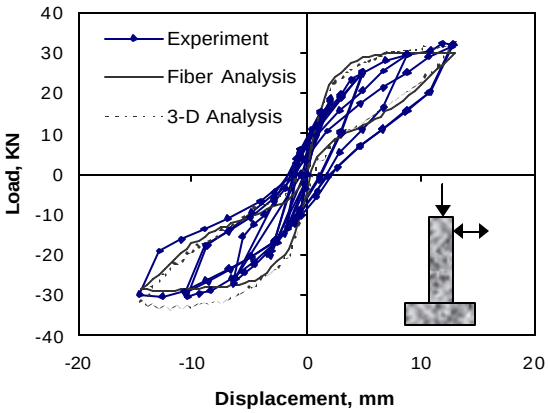

FIGURE 9. Pre-peak response of RC column.

Performance of Proposed Models

For the verification of the proposed models, two columns were tested under cyclic lateral loading. The difference between these two cases is the axial compression only. In one test, a constant axial compression of 250 kN was applied whereas the next column was tested without axial load. The basic test parameters are included in table 3 and the column cross-section is shown in figure 10.

TABLE 3. Experimental parameters

Column cross section	250mm×250mm
Main reinforcement	6 no. D13 bars
Stirrups	D10 @100mm c/c
Cover thickness	30 mm
Axial compression	250 kN, 0 kN
Shear span	1200 mm
Compressive strength, f_c'	29 MPa
Tensile strength, f_t	2.2 MPa
Young's Modulus, E_s	202000 MPa
Yield strength, f_y	360 MPa

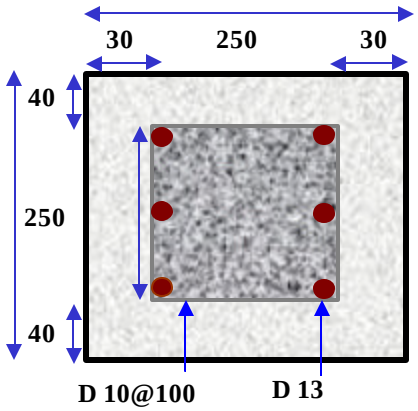

FIGURE 10. Cross-section of specimen.

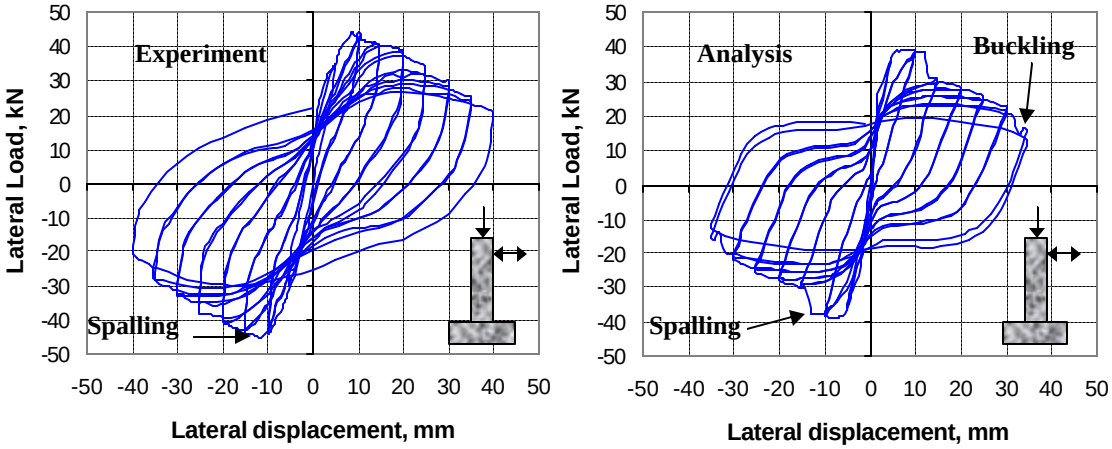

FIGURE 11. Load-displacement relation (with axial compression).

The experimental and analytical load-displacement curves of the column with axial compression are shown in figure 11. In experiment, spalling cracks at the base of the column emerged when the applied displacement reached around 15 mm, which is found to be very close to the analytical prediction. Gradual decrease in the lateral load can be observed after initiation of cover spalling in the experimental result. On the other hand, a sudden decrease in the load is seen in the analytical result. This is because of the spalling model, which abruptly neglects the strength contribution of cover concrete fibers, once the spalling strain is reached. In the analysis, buckling took place during the last loading cycle. However, in experiment, slightly buckled

reinforcements could be observed after scratching out the spalled cover concrete after the experiment. However, the starting point of buckling could not be distinguished. It is found that the analysis could predict the post-peak softening behavior and the analytical result is closer to the experimental result. However, some difference in the peak load can be seen and it is carried over throughout the post peak response.

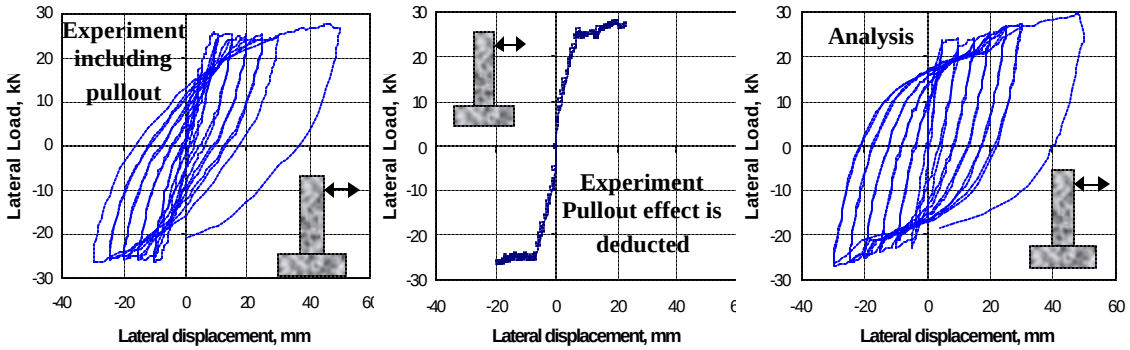

FIGURE 12. Load-displacement relation (without axial compression).

The analytical and experimental results of similar column tested without axial compression are presented in figure 12. As can be observed in the figure, the analytical and experimental results are found to be in good agreement with each other. In the experiment, cover concrete spalling and reinforcement buckling did not take place. In spite of considering the spalling and buckling mechanisms in the analysis, these mechanisms did not occur in analysis, either. The proposed models are based on fiber strain and in this case, the compressive strain in the extreme fiber does not reach the spalling strain. Consequently, softening in the load-displacement relationship was not noticed in the high displacement range, both in experiment and analysis. Analysis without including the proposed models was performed and as expected, similar results were found. This comparison ensures the applicability of proposed models in adverse cases, i.e. where spalling and buckling do not take place.

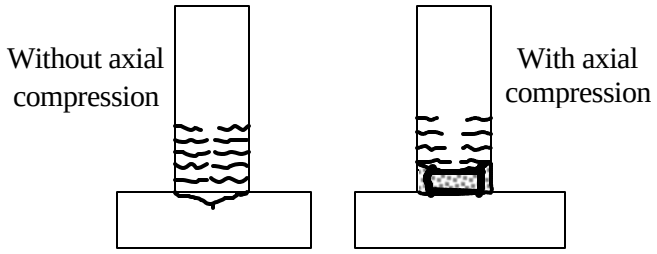

FIGURE 13. Crack pattern at the end of testing.

The final crack pattern in both cases is sketched in figure 13. It is found that the position and spacing of cracks in both cases are exactly the same as those of the lateral ties. In case of columns with small cover thickness, splitting of cover concrete can cause such cracks. But in this case, the clear cover outside lateral ties is more than 15 mm. Hence, the cause of such cracking pattern is still not clear and further

investigation is beyond the scope of this study. As the specimens were designed to have comparatively higher shear strength, no diagonal shear cracks could be seen.

In case of the column without axial compression, inclined cracks initiated from the column footing joint and under cyclic loading these inclined cracks from two sides merged as shown in figure 13. During further loading, these cracks opened and closed significantly. Although other flexural cracks appeared above the column-footing joint, the behavior was mainly governed by these inclined cracks. It might be due to the effect of the joint and the pullout of the main bar. Pullout behavior could also be observed in the experiment. On the other hand, in case of column with axial compression, inclined cracks at the column-footing joint did not emerge. Uniform flexural cracks appeared gradually and the behavior was governed by the crack nearest to the footing. During the cyclic loading, alternate opening and closure of this crack was noticed and after a few cycles, spalling cracks developed. Because of high axial compression, pullout effect was also negligible.

APPLICATIONS OF 3D FEM ANALYSIS ON RC PIERS

High Strength Concrete Column under Lateral Cyclic Load

The application of the proposed models to high strength concrete column is discussed hereafter. Experimental results of lateral cyclic loading tests of circular cantilever reinforced concrete columns with high strength concrete and steel under constant axial compression (150 kN) are considered [Fukui et al. 1998]. Two columns with different reinforcement arrangements are considered. The geometrical and mechanical properties of the columns are explained in table 4 and figure 14.

TABLE 4. Experimental parameters

	Column ***a***		Column ***b***	
	Outer layer	Inner layer	Outer layer	Inner layer
Diameter	300 mm	180 mm	300 mm	180 mm
Main reinforcement	12 no. D7 bars	_	12 no. D7 bars	16 no. D10 bars
Stirrups	D6 @50mm	_	D3 @50mm	D6 @75mm
Cover thickness	30 mm	_	30 mm	30 mm
Comp. strength, f_c'	82.6 MPa	28 MPa	81.1 MPa	27.4 MPa
Tensile strength, f_t	3.9 MPa	2.6 MPa	4.8 MPa	2.4 MPa
Young's Modulus, E_s	2.06E5 MPa	_	2.06E5 MPa	1.79E5 MPa
Yield strength, f_y	1538 MPa	_	1538 MPa	354.7 MPa

Both columns constitute of two layers of concrete with different strengths. The inner core consists of normal strength concrete whereas the peripheral (outer) layer consists of high strength concrete. Column *a* includes high strength reinforcement in the outer layer. On the other hand, column *b* has two layers of reinforcement, i.e. high strength reinforcement in the outer layer and normal

reinforcement in the inner layer. Consequently, the reinforcement ratio of column *a* is significantly smaller than that of column *b*. The cover thickness is the same in both columns. In both columns, spiral reinforcement is used for the outer layer of longitudinal reinforcements. But for analytical convenience, they are treated as circular hoops with spacing equal to the pitch of the spiral reinforcement.

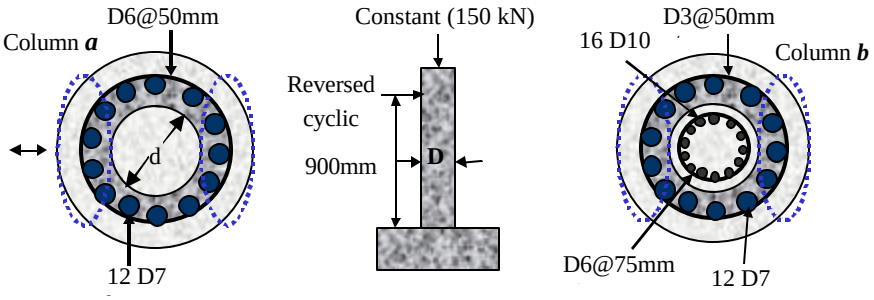

FIGURE 14. Column cross-sections and test setup.

The experimental results and analytical responses obtained by fiber technique, with and without including proposed spalling and buckling models, are illustrated in figure 15. Only the envelope curves are shown in the figure. The cyclic behavior in the analysis was different from the experimental cyclic response, notably the cyclic loops were larger and the residual displacement was higher in analysis. This might be because of the cyclic model used for the reinforcement, which adopts the Young's modulus for unloading and reloading stiffness regardless of the absolute strain experienced in the loading history. Here, the discussion is mainly focussed on the response envelope (peak points of the cyclic loops).

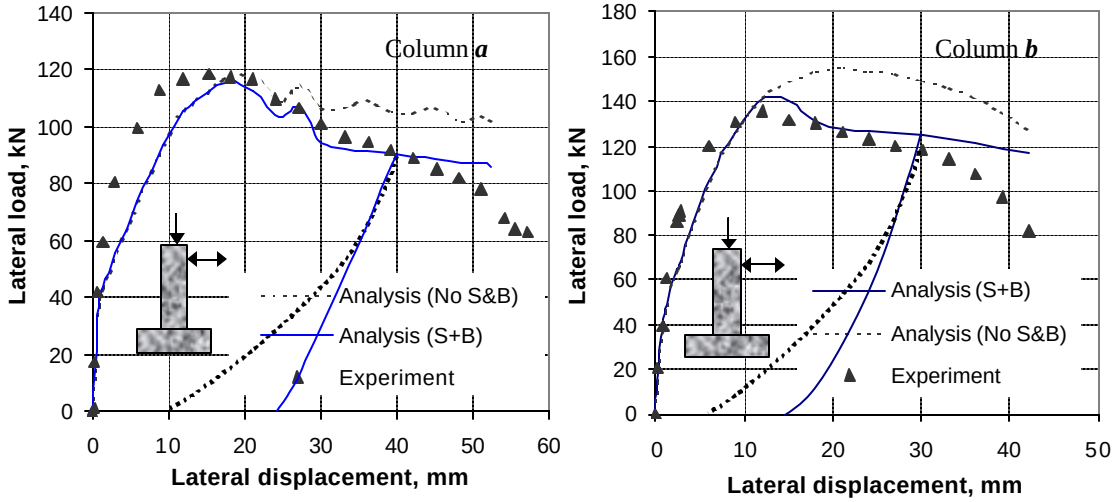

FIGURE 15. Post-peak response envelop.

As can be seen from the figure, the peak load of column *b* is higher than that of column *a* and the post peak response of column *b* is relatively flatter and comparatively milder softening is observed. The additional resistance comes from the inner layer of reinforcement. Even after the yielding of the outer reinforcement in

column *b*, the inner reinforcements are still behaving elastically. As a result, the post peak softening is comparatively milder. It is to be noted that these inelastic material mechanisms influence only the post peak response of column *a* but interestingly, peak load is also influenced in case of column *b*. Ultimately, in both cases, the analysis including the proposed models could predict the behaviors that are very close to the reality (experimental results). Conclusively, it can be said that the proposed analytical models can reliably predict the overall behavior of high strength columns, including the peak load and post-peak response.

Eccentrically Loaded RC Bridge Piers Subjected to Ground Motion

In order to verify the applicability of proposed models in dynamic analysis, the result of a shaking table test of reinforced concrete column, eccentrically loaded in axial compression, is adopted [Kawashima et al. 1995]. The details and dimensions are explained in figure 16.

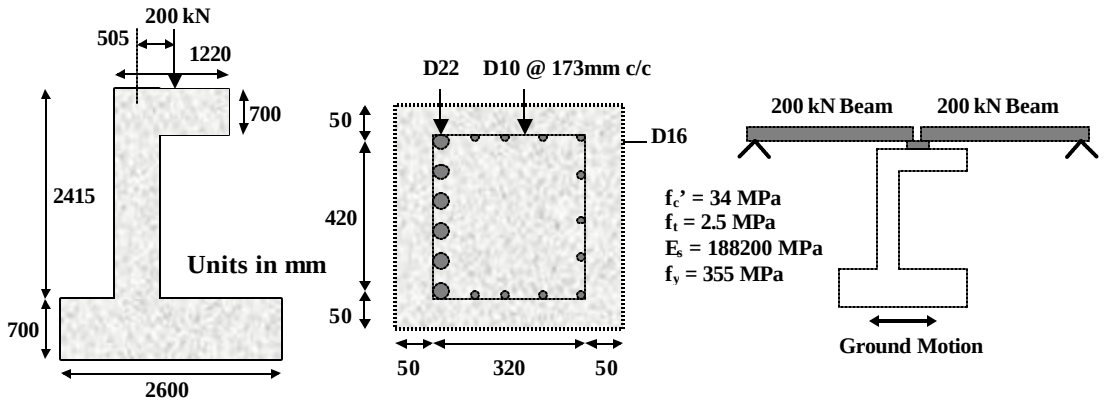

FIGURE 16. Experimental layout and specimen details.

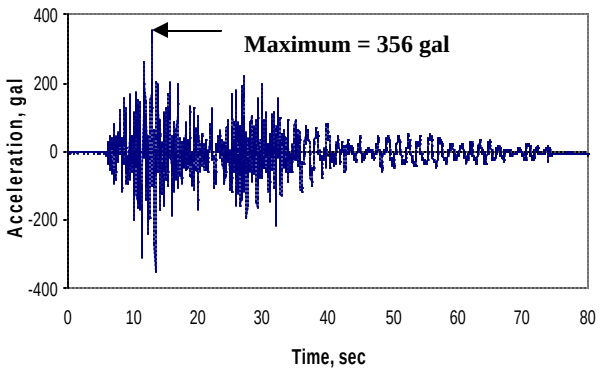

FIGURE 17. Base acceleration used in experiment.

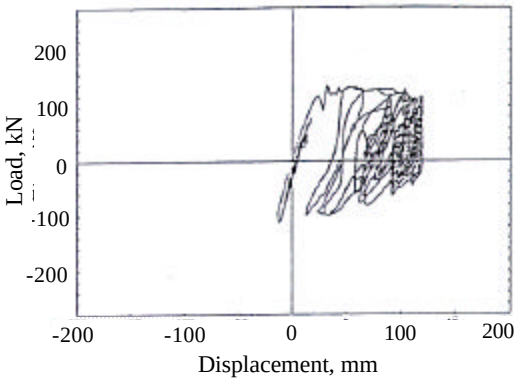

FIGURE 18. Hysteresis loop (Experiment).

The specimen consists of a rectangular reinforced concrete column fixed to a shaking table with a rigid footing. A superstructure consisting of two 200kN beams is eccentrically supported at the top of the column, as shown in the figure. Base acceleration, similar to Nihonkai-Chubu Earthquake in 1993, is applied to the base of

the column through the shaking table. The time history of the base acceleration used in the experiment and fiber analysis is depicted in figure 17.

The experimental result, i.e. the relationship between the base shear and the displacement at the top of the column, is demonstrated in figure 18. From the curve shown above, it can be guessed that there must be some technical or instrumental problems in measuring displacement greater than 130 mm during the experiment. Hence, the higher displacement could not be recorded and the load-displacement relationship in the later part is perfectly vertical, which does not reflect the actual behavior. Hence, the final values of maximum and residual displacements are expected to be more than as shown in the figure.

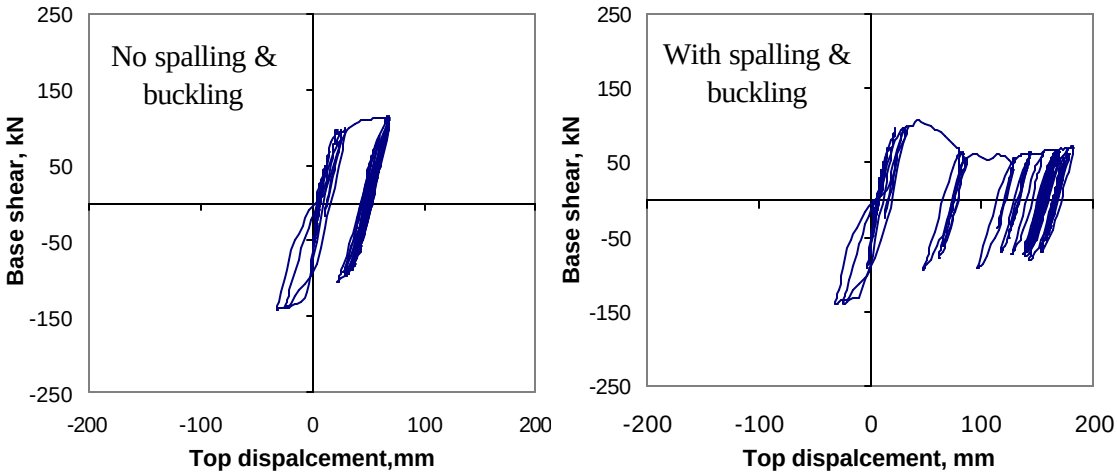

FIGURE 19. Hysteresis loop (Analysis).

The results of the fiber analysis with and without using the proposed spalling and buckling models are given in figure 19. In the analysis, geometrical nonlinearity was incorporated in order to include the P-delta effect. However, it was found that the effect of geometrical nonlinearity was not so significant because the maximum response predicted by conventional fiber models was very small (around 70 mm). As can be distinguished from the result, the residual displacement and ductility are underestimated if spalling and buckling mechanisms are not included. This result, if used for performance based seismic design, may lead to unsafe structures that might experience larger deformation during actual ground motion. On the other hand, the analytical results obtained by using proposed models are closer to reality. As the final value of residual displacement in experiment is not clearly known, exact comparison between the two results cannot be done. However, it can roughly be said that these enhanced analytical models yield more reliable results, which predict the ductility and residual displacement to be at least equal to or more than the experimental values. In both cases, the performance of the designed structure can be ensured, although it might be slightly conservative.

Box Type Hollow RC Columns under Cyclic Torsion, Shear and Bending

3D FEM analysis using *shell element* has been carried out for verification of the analytical tool for complex loading. Figure 20 shows the analysis and results of a box type hollow RC column under cyclic torsion, shear and bending load [Masukawa et al. 1999]. The computed bending moment-curvature and torque-twist relationships are compared with the experimental data. The computational tool can effectively predict the deformation and stiffness by shear and bending. However for the torsion, the post-cracking stiffness and ultimate capacity are considerably higher than experimental results, as the cover concrete spalling occurred in reality due to torsion. This torsion resistance reduction caused by spalling must be addressed in the near future.

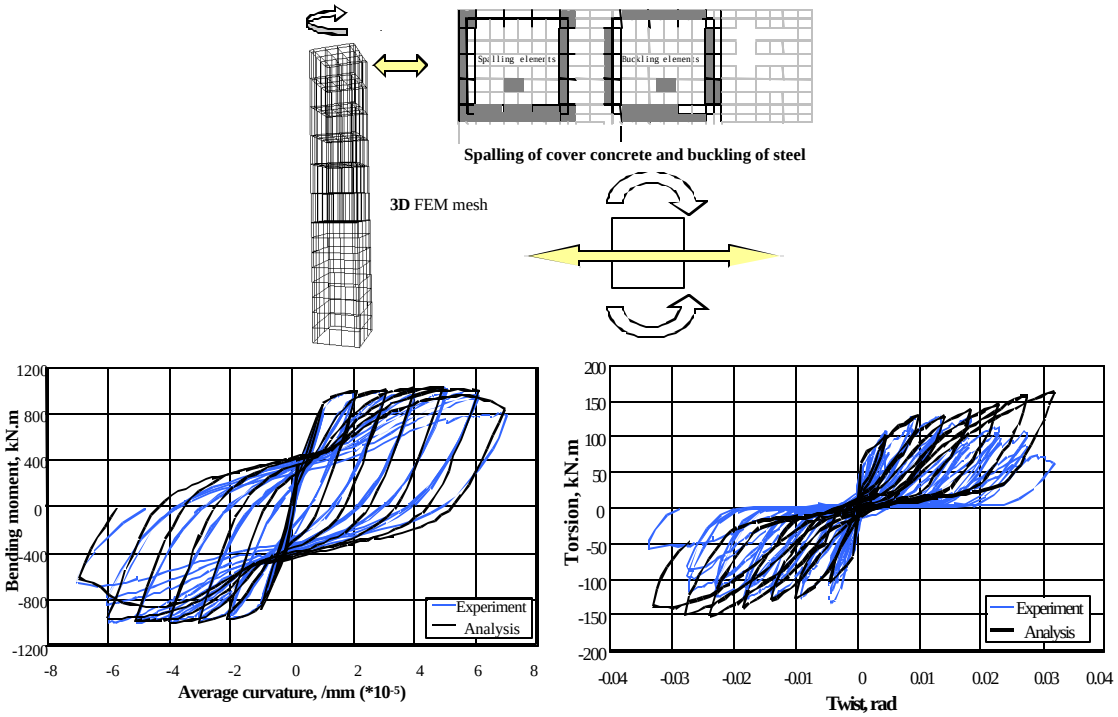

FIGURE 20. Analysis of hollow RC columns under cyclic torsion, shear and bending.

Solid RC Columns under Cyclic Torsion, Shear and Bending

Furthermore, a solid RC column under combined cyclic torsion, shear and bending is analyzed using 3D *solid elements.* The proposed spalling and buckling models are not included in the material models used in this analysis. Three-dimensional cracks in all directions are observed inside the column during the experiment. In figure 21, the analytical results are compared with the experimental data [MEPC 1997]. The computed horizontal force has been over estimated in the inelastic region, which is attributed to the cover concrete spalling and reinforcement buckling. Hence, these mechanisms should be incorporated in 3D analysis to reliably predict the post-peak behavior of such structures.

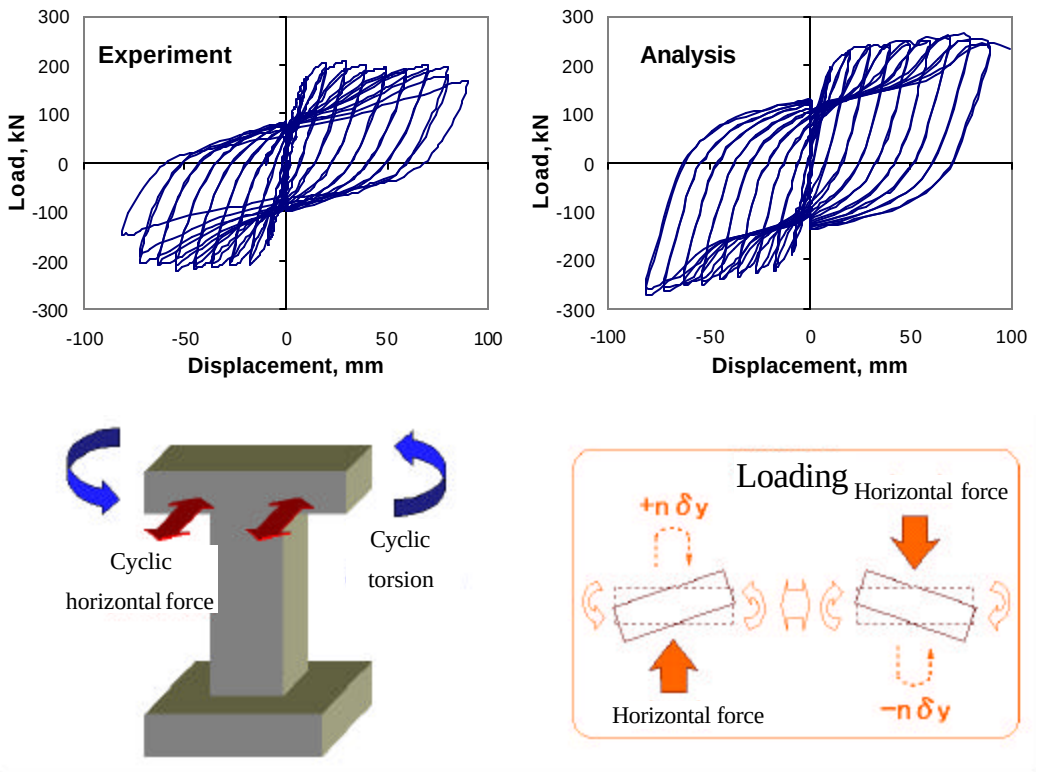

FIGURE 21. Simulation of solid RC columns under cyclic torsion, shear and bending.

RC Short Columns Subjected to Bi-axial Shear

Here, short RC columns [Yoshimura 1996] are used for verification of the full 3D non-linear analysis frame. A constant axial load (1500 kN) and fixed horizontal load in Y-direction (0, 150, 250, 350 kN for different specimens) are applied. After setting these forces, varying enforced displacement in X-direction normal to the already applied shear is monotonically applied until failure. The reinforcement details and layout of the specimens are shown in figure 22. Under this load application scheme, spatial development of stress induced cracks is irregular due to the complexity of stress field unlike reinforced concrete of 2D in shear. In such cases, it is realised that isotropic tension stiffening overestimates the actual load capacity and anisotropic tension softening is taken into account [Hauke 1998].

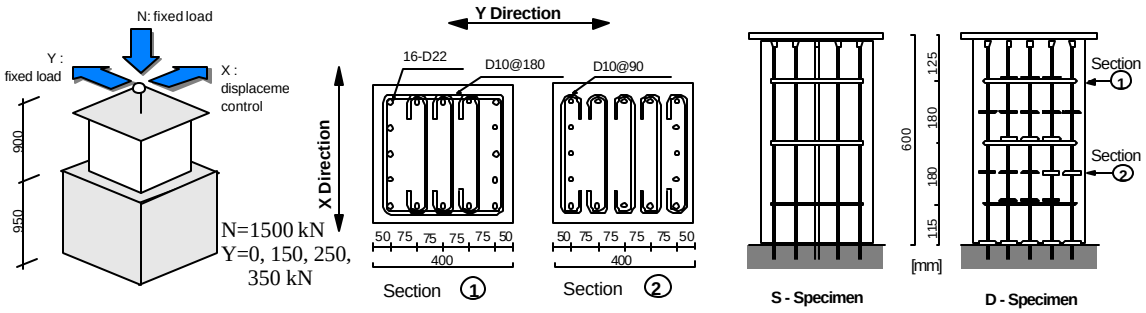

FIGURE 22. Setup and reinforcement layout of short RC column loaded in bi-axial shear.

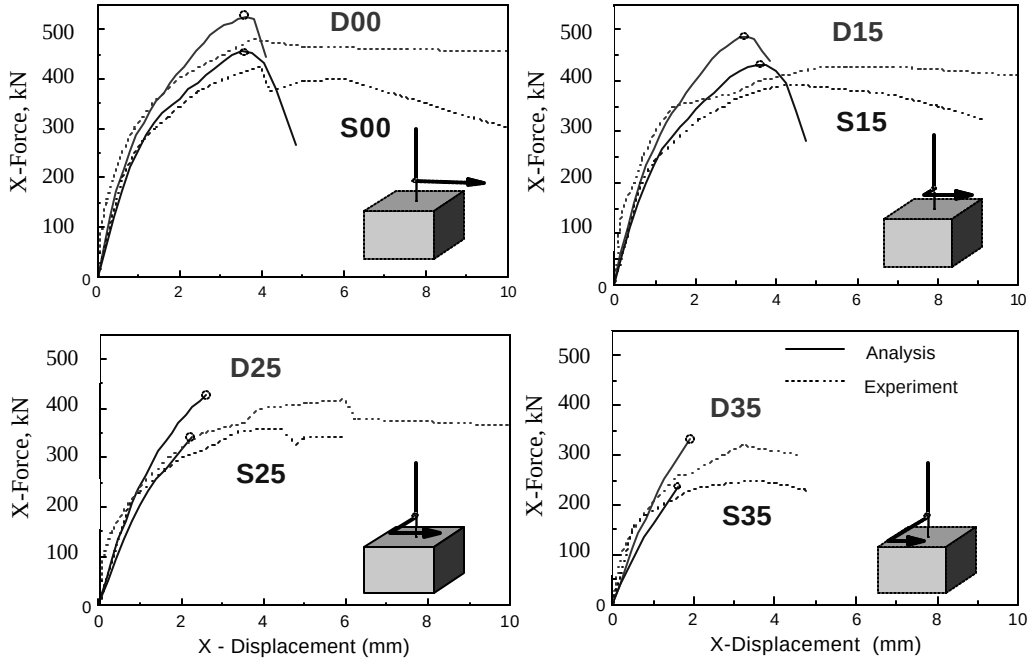

FIGURE 23. Bi-axial shear load-displacement diagram (X-direction).

In figure 23, the experimental and the computed X-load - X-displacement curves are plotted. As the level of pre-imposed Y-load increases, the initial stiffness in X-direction decreases in computation due to pre-accumulated damage. The influence of the additional hoops in X-direction, improving stiffness and ultimate shear capacity in that direction is qualitatively and correctly reflected in analysis. Up to the peak of load displacement diagrams, full 3D constitutive models work well with reasonable accuracy for engineering purposes. Nevertheless, in the post peak range of the response, computation is not successful.

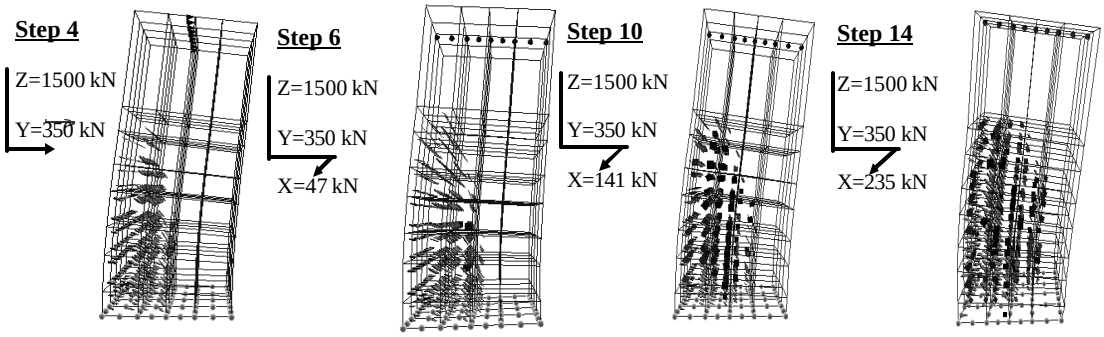

FIGURE 24. Evolution of 3D inclined variable cracks under multi-directional loading (S35).

Using a graphical tool based on **V**irtual **R**eality **M**odelling **L**anguage [Takahashi and Maekawa 1998], step by step development of predominant 3D variably inclined cracks for specimen S35 is obtained as shown in figure 24. In step 1, axial compressive load of 1500kN is applied and naturally no cracks can be found. In

step 2 to 4, fixed horizontal Y-force is applied and after full Y-force is applied in step 4, typical inclined shear cracks develop. As Y-direction is kept clamped and displacement controlled load is applied in the perpendicular X-direction from step 5 onwards, final shear failure plane is slowly changed from the originally induced shear crack plane. Here, the full three-dimensional inclined shear plane can be clearly identified.

Conclusions

Based on the experimental facts of bare bar compression tests with local geometrical nonlinearity, an analytical model relating the averaged compressive stress and compressive strain of the reinforcement is proposed. Coupling this monotonic stress-strain relationship with tension envelope and Giuffre-Menegotto-Pinto model for unloading and reloading formulate a cyclic stress-strain relationship. Both for monotonic and cyclic cases, the proposed model showed fair agreement with the experimental results of bare bar tests. Based on the interaction with cover concrete spalling and the geometrical and mechanical properties of the lateral reinforcements, the behavior of longitudinal reinforcements in compression was revised. Finally, versatile models for the spalling of cover concrete and buckling of reinforcement in reinforced concrete members were proposed. A design method was also proposed in terms of the lateral ties against the buckling of main bar. The proposed models were included in a finite element analysis program, COM3, and its applicability to various types of reinforced concrete structures was investigated.

As expected, it was discovered that the existing material models without considering spalling and buckling phenomena could fairly predict the pre-peak response of reinforced concrete structures. However, the post peak-response and in some special cases peak load, too, were found to be influenced by these material and geometrical nonlinearities. The proposed models were used to analyze normal and high strength reinforced concrete columns under cyclic and seismic loading. In all cases, significant improvement in the prediction of overall response could be achieved by using proposed models. However, the effect of these mechanisms in the torsion resistance of RC piers needs further attention in future. Furthermore, the applicability of 3D nonlinear analysis tool was verified for non-proportional biaxial shear loading of short RC columns and the irregular rotation and propagation of the cracks were also studied.

References

Bresler, B. and Gilbert, P. H. (1961). "Tie Requirements for Reinforced Concrete Columns." *Journal of ACI*, 58 (5), 555-570.

CEB (1996). *RC Elements under Cyclic Loading - State of the Art Report*, Thomas Telford.

Dhakal, R. P. and Maekawa, M. (1999). "Behavior of Laterally Loaded RC Columns with Thick Cover under Axial Compression." *Proc. of JSCE Annual Conference*, Hiroshima.

Fukui, J., Nakano, M., Kimura, Y., Ishida, M., Okoshi, M. and Sakano, A. (1998). "Loading Tests about the Ductility of Pile Foundations." *Technical Memorandum of PWRI*, No. 3553 (Japanese).

Gomes, A. and Appleton, J. (1997). "Nonlinear Cyclic Stress-Strain Relationship of Reinforcement Bar Including Buckling." *Engineering Structures*, 19 (10), 822-826.

Hauke, B. (1998). "Three-Dimensional Modeling and Analysis of Reinforced Concrete and Concrete Composites." *Doctoral Thesis*, University of Tokyo.

Kato, D., Kanaya, J. and Wakatsuki, K. (1995). "Buckling Strains of Main Bars in Reinforced Concrete Members." *Proceedings of the EASEC-5*, Australia, 699-704.

Kawashima, K., Unjou, S., Nagashima, H., Iida, H. and Mukai, H. (1995). "An experimental Study on Seismic Resistance and Seismic Performance of RC Piers Subjected to Eccentric Loading." *Technical Memorandum of PWRI*, No. 3319 (Japanese).

Masukawa, J., Suda, K. and Maekawa, K. (1999). "3-Dimensional Nonlinear FEM Analysis of Hollow Bridge Piers Considering Spalling of Concrete Cover and Buckling of Reinforcing Bars." *Proceedings of the Japan Concrete Institute*, 21 (3), 37-42.

Mau, S. T. (1990). "Effect of Tie Spacing on Inelastic Buckling of Reinforcing Bars." *ACI Structural Journal*, 87 (6), 671-678.

Mau, S. T. and El-Mabsout, M. (1989). "Inelastic Buckling of Reinforcing Bars." *Journal of Engineering Mechanics*, 115 (1), 1-17.

Metropolitan expressway public corporation (1997). *Report of experiment results of bridge piers under torsion and bending loads*.

Monti, G. and Nuti, C. (1992). "Nonlinear Cyclic Behavior of Reinforcing Bars Including Buckling." *Journal of Structural Engineering*, 118 (12), 3268-3284.

Okamura, H. and Maekawa, K. (1991). *Nonlinear Analysis and Constitutive Models of Reinforced Concrete*, Gihodo.

Rodriguez, M. E., Botero, J. C. and Villa, J. (1999). "Cyclic Stress-Strain Behavior of Reinforcing Steel Including Effect of Buckling." *Journal of Structural Engineering*, 125 (6), 605-612.

Scribner, C. F. (1986). "Reinforcement Buckling in Reinforced Concrete Flexural Members." *ACI Journal*, 1986 (6), 966-973.

Suda, K. (1998). *Ductility Study of Long and Hollow Reinforced Concrete Columns*, Doctoral Thesis, University of Tokyo (Japanese).

Suda, K., Murayama, Y., Ichinomiya, T. and Shimbo, H. (1996). "Buckling Behavior of Longitudinal Reinforcing Bars in Concrete Column Subjected to Reverse Lateral Loading." *Eleventh World Conference on Earthquake Engineering*, No. 1753.

Takahashi, T. and Maekawa, K. (1998). "Visualisation of Three Dimensional RC Crack Analysis using Immersive Multi-Screen Display." *Proc.of JCI*, 20 (1), 149-154 (Japanese).

Yoshimura, M. (1996). "Failure Envelope of RC Columns in Two-Way Shear." *Summaries of Technical Papers of Annual Meeting*, AIJ, 199-200 (Japanese).